Chemical Stratigraphy of the Windsor Group Marine Sediments, Shubenacadie Basin, Nova Scotia

Carmen A. Braun

Submitted in partial fulfillment of the requirements for the degree of Bachelor of Science, Honours
Department of Earth Sciences
Dalhousie University, Halifax, Nova Scotia

Distribution License

DalSpace requires agreement to this non-exclusive distribution license before your item can appear on DalSpace.

NON-EXCLUSIVE DISTRIBUTION LICENSE

You (the author(s) or copyright owner) grant to Dalhousie University the non-exclusive right to reproduce and distribute your submission worldwide in any medium.

You agree that Dalhousie University may, without changing the content, reformat the submission for the purpose of preservation.

You also agree that Dalhousie University may keep more than one copy of this submission for purposes of security, back-up and preservation.

You agree that the submission is your original work, and that you have the right to grant the rights contained in this license. You also agree that your submission does not, to the best of your knowledge, infringe upon anyone's copyright.

If the submission contains material for which you do not hold copyright, you agree that you have obtained the unrestricted permission of the copyright owner to grant Dalhousie University the rights required by this license, and that such third-party owned material is clearly identified and acknowledged within the text or content of the submission.

If the submission is based upon work that has been sponsored or supported by an agency or organization other than Dalhousie University, you assert that you have fulfilled any right of review or other obligations required by such contract or agreement.

Dalhousie University will clearly identify your name(s) as the author(s) or owner(s) of the submission, and will not make any alteration to the content of the files that you have submitted.

If you have questions regarding this license please contact the repository manager at dalspace@dal.ca.

Grant the distribution license by signing and dating below.

_____ _____

Name of signatory Date

Abstract

This study examines a section of core from the Windsor Group in order to reconstruct paleoclimatic conditions at the time of deposition. In restricted marine basins, evaporite deposits form consistent and recognizable sequences. The typical order of precipitation and deposition in these sequences is carbonates first, sulphates second, halites third, and other salts last. In a partially or periodically restricted basin with evaporative conditions, this sequence will start anew with each new marine transgression, which leads to cyclical evaporite deposits. The Maritimes Basin (mid-Devonian to Permian) records continuous deposition, including that of the Windsor Group. Deposited during the Visean, it is the only marine sequence in the basin; it is comprised primarily of cyclic evaporite deposits. These deposits will include different trace and minor elements. Trace element ratios, such as Mg/Ca, Ba/Ca, and Sr/Ca, can be important indicators of paleo ocean conditions, including temperature. For example, the ratio of Mg to Ca will go up, while those of Ba and Sr to Ca will go down when the temperature of the ocean increases. Isotopic records can also serve as temperature proxies. However, diagenesis is more likely to affect isotopic ratios than elemental ratios. The presence of Fe is a good indicator of diagenesis, since it is present only in very low concentrations in normal seawater.

Analysis methods in this study include visual observations of core, hand sample, and thin section, as well as electron microprobe and x-ray fluorescence analyses of the thin sections and hand samples respectively. Fe-rich zones around anhydrite nodules and Fe in the dolostone show that there has been some diagenesis. If this diagenesis occurred in a rock-dominated system, it will have preserved the elemental ratios. The ratio of Mg/Ca is highly variable, on the foot scale, from 1600 to 1450 ft depth, above which scale of the variations increases. The ratio decreases overall until 1150 ft, where it begins to increase. Above 750 ft, it begins to decrease again. The ratios of Ba/Ca and Sr/Ca are also highly variable below 1450 ft, and less so above. Above that point, the ratios trend inversely compared to Mg/Ca. The variability in the ratios on the smaller scales corresponds well to previously identified transgressive-regressive cycles. The longer scale trends suggest oceanic cooling during deposition of the material from 1450 to 1150 ft (336.3-335.3 Ma) and 725 ft to the top of the study section (331.5-330 Ma), and warming between 1150 and 725 ft (335.3-331.5Ma). The overall increasing trend in Mg/Ca ratios correspond to previous studies. Further study is required to determine the conditions under which diagenesis occurred.

Keywords: evaporites, carbonates, element ratios, Windsor Group, paleoclimate, ocean temperature, Visean

Table of Contents

Abstract II

Table of Figures II

Acknowledgements III

Chapter 1 - Introduction 1

Chapter 2 - Background 4

Geology of the Maritimes Basin 4

Windsor Group 5

Core SB-1 8

Chapter 3 - Methods 9

Core Description 9

Polished Sections – Petrographic Descriptions 10

Microprobe Analysis 10

X-Ray Fluorescence (XRF) 11

Chapter 4 – Results 12

Sample Descriptions 12

Microprobe Data 16

XRF Data 20

Chapter 5 – Discussion 25

Diagenesis 25

Seawater History 26

Mg/Ca 26

Ba/Ca 27

Sr/Ca 28

Conclusions 28

References 30

Appendix 34

Appendix A: Sample Descriptions and Locations 34

Table of Figures

Figure 2-1 The location of the Maritimes Basin and of Core SB-1 5
Figure 2-2 Lithostratigraphy of core SB-1 with limestone/dolostone members labled 6
Figure 3-1 Photo of core from 1035-1120 ft depth. 9
Figure 3-2 Photo of sample CB-48, a coarse nodular anhydrite with a silty dolostone matrix 10
Figure 4-1 Core log with member and sample locations. 13
Figure 4-2 Photos of common textures in hand sample 14
Figure 4-3 Representatice thin section scans 15
Figure 4-4 Graph of Fe and Mg content against Ca content in all dolostone, sulphates, and in the calcite standard 17
Figure 4-5 X-ray map of mixed dolostone and sulphate 18
Figure 4-6 X-ray map of bedding in a dolostone (top is to the right) 19
Figure 4-7 X-ray map of chicken-wire texture in sulphate 19
Figure 4-8 X-ray map of Fe content in a fossiliferous and bedded dolostone 20
Figure 4-9 XRF data for Mg, Ca, Fe, S, Ba, Sr, Si, and Mn 22
Figure 4-10 XRF element ratio data for all sample points in ppm. 23
Figure 4-11 XRF data for the sulphates or dolomites only. 24

Acknowledgements

I would like to thank everyone who helped me throughout the year including Mick O'Neill at the NS Core Library for helping me move endless pallets and boxes of core. Thanks to Gordon Brown for creating thin sections. Special thanks to Dan MacDonald in the microprobe lab for putting up with me and my issues with scheduling. Thanks to Ricardo Silva for setting up the XRF analyses, and Phillip Sedore for doing them all. Thanks also to my supervisor, Richard Cox.

I would also like to thank my friends, family, and other professors who have been so very supportive and encouraging.

Chapter 1 - Introduction

This study will focus on the late-Visean marine sequences deposited in Nova Scotia that form the Windsor Group in an effort to characterize the chemical stratigraphy and determine paleoclimatic changes in the section. This is the only marine-dominated group deposited in the Maritimes Basin and therefore represent a unique opportunity to investigate local paleo-oceanic conditions.

Seawater contains many ions that will begin to precipitate out of solution when they become supersaturated. This occurs principally when the evaporation rate exceeds water inputs, and is particularly pronounced in restricted basins where solute content of the source water is higher than in open oceanic basins [*Lugli*, 2009]. In marine environments, the combination of restricted marine basins and low water input are most likely to occur where warm conditions and closed off basins or inland seas are prevalent [*Lugli*, 2009; *Boggs*, 2012]. In such environments, the precipitating ions will form a sequence of evaporite minerals. In evaporite sequences, the first mineral to precipitate is calcium carbonate ($CaCO_3$). Carbonate precipitation begins when about 50 percent of seawater has evaporated [*Boggs*, 2012]. As evaporation continues, the evaporite group minerals will begin to precipitate in sequence. When about 15 percent of seawater remains, gypsum/anhydrite ($CaSO_4 \pm 2H_20$), the first in the evaporite mineral sequence, begins to precipitate. When only 10 percent remains, halite (NaCl) precipitates, followed by variable potassic salts [*Lugli*, 2009; *Boggs*, 2012]. Barring any intermittent water inputs, the majority (78 percent) of the resultant deposit will be halite, and the depth of the entire deposit will be about 1.4% of the original seawater depth [*Lugli*, 2009]. However, in situations where there are periodic seawater inputs after mineral precipitation and deposition has occurred, much thicker deposits can form.

Periodic marine inputs, such as successive transgressive-regressive cycles, produce

repetitive depositional sequences [*Allen et al.*, 2013]. In an evolving basin, this can lead to variable carbonate and evaporite rock sequences interspersed with clastic sediments. If there is terrigenous material in a sequence, it will be most abundant at the transition between cycles, and the carbonates and the evaporite mineral sequence will follow further marine input. This new marine input will reset the system and seawater precipitation will continue. Successive marine inputs can indicate transgressive-regressive cycles [*Giles*, 2009]. Thus, variation in these sequences can be an indication of geological and paleo-environmental changes over both long (several million years) to moderately short (several thousand years) time scales.

Throughout this type of sedimentary sequence, environmental and geological conditions will affect the crystals forming directly from seawater as they incorporate minor and trace elements present in the concentrated solution. For example, Sr^{2+} replaces both Ca^{2+} and Ba^{2+}, and Ba^{2+} replaces Ca^{2+} in carbonates and sulphates [*Salminen*, 2005]. The rate at which they will do so is a function both of the rate of mineral precipitation and the concentration of the element in the original seawater [*Rimstidt et al.*, 1998]. These rates, while they have been theoretically and experimentally derived, are highly variable in natural systems [*Morse and Bender*, 1990]. Therefore, it is vital to characterize the sequences properly before analysis. In addition, it is useful to use and compare the ratio of these elements, instead of using their absolute concentrations [*Cicero and Lohmann*, 2001]. For example, the Sr/Mg ratio in the precipitate is linear and depends on the concentration of Mg in solution [*Carpenter and Arbor*, 1992; *Cicero and Lohmann*, 2001]. In the case of Mg and Ca, the precipitate incorporates more Mg at higher temperatures due to changes in the kinetic mechanisms whereby crystal comparison growth becomes more disordered [*Lopez et al.*, 2009]. The Mg/Ca ratio of the seawater will also affect the Mg/Ca ratio in the precipitate; however, changes in saturation, or salinity, do not [*Lopez et al.*, 2009; *Hasiuk and Lohmann*, 2010]. Conversely, the ratios of Sr/Ca and Ba/Ca decrease at

higher temperatures [*Shen et al.*, 1996; *Gornitz*, 2009; *Cohen and Gaetani*, 2010]. The relationship between the Mg/Ca, Sr/Ca, and Ba/Ca ratios and temperature means evaporite deposits can reflect changes in the paleo-temperature of the ocean from which they precipitated.

The residence times of Mg, Ca, Ba, and Sr in the ocean are around 10 Ma, 1 Ma, 84 ka, and 2.5 Ma respectively [*Hem*, 1985; *Andreasen and Delaney*, 2006]. These are all much longer than the mixing time of the modern ocean (~1 ka). While the Cretaceous mixing time was probably longer, based on the global climate and paleogeography, it still would have been of a similar scale. Therefore, the ratios of all will have been homogeneous in the open ocean.

After precipitation from seawater, where temperature and element concentrations will determine the initial amounts of a given element in the mineral, diagenesis can cause alterations. Diagenesis can also affect primary textures, elemental concentrations, and isotopic ratios in marine carbonates [*Al-Aasm and Packard*, 2000]. For example, Fe and Mg are present in much higher concentrations in groundwater than in seawater; passage of groundwater through evaporite deposits can alter the amount of Fe and Mg in those deposits [*Moore*, 1989; *Morse and Mackenzie*, 1990]. Due to this, it is important to characterize the minerals within these sequences carefully, in order to determine whether they reflect the primary seawater crystallization.

In summary, marine depositional sequences can provide evidence of many geologic processes. Such processes include changes in the transgression-regression rates, and temperature and composition of paleo-seawater. They can also show evidence of diagenetic changes during lithification and, therefore, the longer-term evolution of the sedimentary basin. A recent study of primary fluid inclusions within two halite sections from the middle of the Windsor Group evaporites sought to establish the seawater composition for this geological time period [*Holt et al.*, 2014]. The data from Holt et al. (2014) will act as a source of comparison with the data in the present study.

Chapter 2 - Background

Geology of the Maritimes Basin

After the Laurentia-Gondwana collision, which occurred during the formation of Pangea, strike-slip faults and deformation continued; this resulted in the formation of the Maritimes Basin [*Murphy et al.*, 2011]. See Figure 2-1 for the location of the basin deposits in relation to Atlantic Canada. The Maritimes Basin was tectonically active from the Mid-Devonian to the Permian [*Gibling et al.*, 2008; *Murphy et al.*, 2011]. The Maritimes Basin is a composite, intracontinental basin that encompasses several smaller basins, including the Shubenacadie Basin. The basins formed from continental graben fills, in an extensional step-over zone [*Jutras et al.*, 2006; *Hibbard and Waldron*, 2009]. The subbasins are generally northeast trending and follow the basement fault blocks [*St. Peter*, 1993]. The Maritimes Basin covers much of northwestern Nova Scotia, as well as P.E.I., eastern New Brunswick, and parts of Newfoundland [*Schenk et al.*, 1994; *Gibling et al.*, 2008; *Allen et al.*, 2013]. The preserved Maritimes Basin sediments are up to 13 km thick in some regions [*Schenk et al.*, 1994; *Calder*, 1998; *Allen et al.*, 2013] and cover an area of 148000 km^2 overlying five deformed basement terranes [*St. Peter*, 1993]. The sediments accumulated when the region was near the equator [*Gibling et al.*, 2008]. The sediments are nearly continuous and all terrestrial, except for a period in the mid-late Visean (330.9–346.7 Ma) when a marine transgression occurred due to thermal subsidence [*Calder*, 1998; *Gibling et al.*, 2008]. Deposition of the marine sediments began in deeper water that rapidly became more shallow [*Holt et al.*, 2014]. These marine sediments make up the Windsor group.

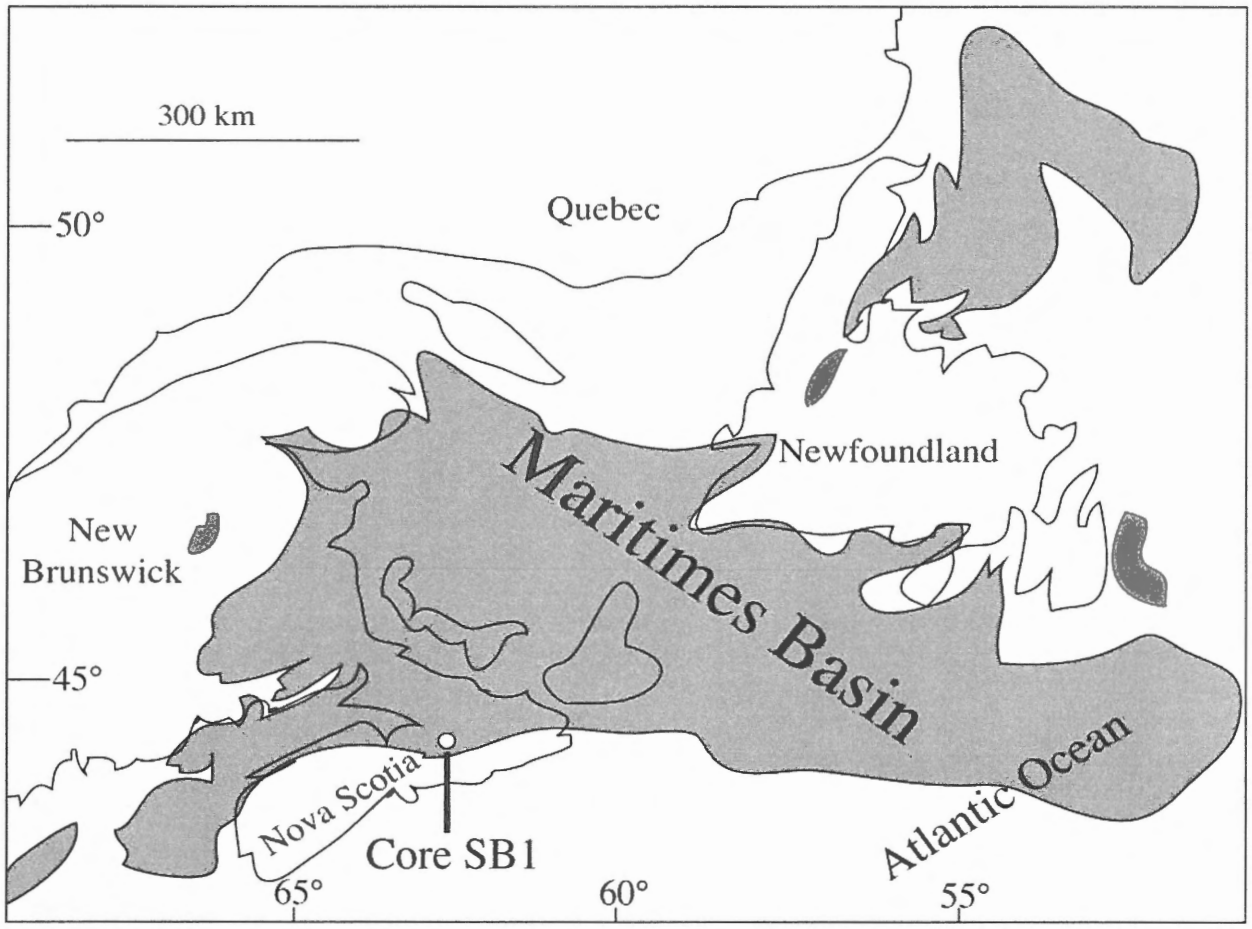

Figure 2-1 The location of the Maritimes Basin and of Core SB-1. Figure modified from Holt et al. [2014]

Windsor Group

The Windsor Group's lithology represents a marked departure from the rest of the basin sediments; it is the only open-marine unit in the basin [*Gibling et al.*, 2008]. It unconformably overlies most of the Horton Group, but overlies the Cheverie Formation of the Horton Group conformably [*Boehner*, 1986; *Gibling et al.*, 2008]. The group becomes more deformed towards the N and NW. In most areas it is ~1 km thick [*Gibling et al.*, 2008]. Giles (2009) describes the late Visean as a cold period, based on a relative lack of sea-level high-stand deposits in the rock record for that time. The Windsor Group is predominantly cyclic anhydrite, halite, fossiliferous carbonate, and dolostone, with some silt- and sandstones; these are representative of the transgressive-regressive cycles that the area experienced [*Giles*, 2009]. Giles (2009), suggested

that orbital forcings accounted for the cyclical evaporite deposits. There are five major transgressive-regressive cycles and fourteen named limestone/dolostone members within the Windsor Group [*Giles*, 1981]. Figure 2-2 shows these cycles as they relate to the different groups and formations, and includes the stratigraphy of the core used in this study.

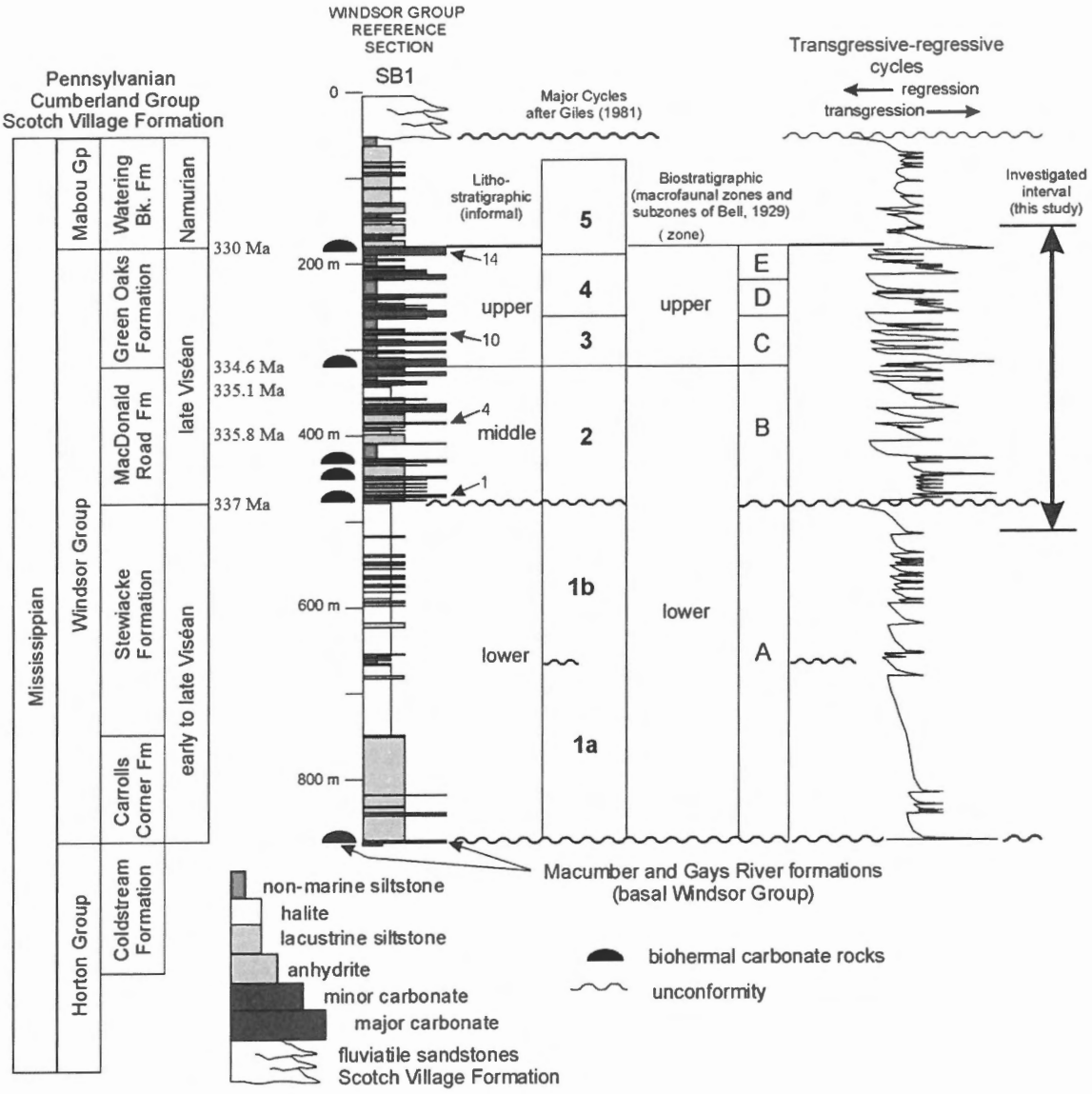

Figure 2-2 Lithostratigraphy of core SB-1 with limestone/dolostone members labled, modified from Giles [2009], with dates from Holt et al. [2014]

Cycle 1 comprises six of the formations within the Windsor Group, including the Stewiacke Formation. These formations are not all laterally continuous. The base of this cycle

corresponds to the earliest marine incursion in the Visean [*Giles*, 1981]. As such, the oldest rocks in the cycle are primarily limestones. These are followed by limestone breccia, then sandstone and shale, or dolostone. It is then overlain by thick anhydrite and gypsum [*Giles*, 1981]. Overlying this is the Stewiacke Formation, which consists of thick (up to 300 m) halite deposits. These halites are massive at the base, with thin interbedded anhydrites mid-section, and interbedded siltstones in the upper portion [*Boehner*, 1986].

The MacDonald Road Formation records the second cycle. Cycle 2 has alternating gypsum/anhydrites and carbonate (limestone or dolostone) rocks, with some fine grained terrigenous sedimentary rocks [*Giles*, 1981]. It encompasses six of the fourteen named limestone/dolostone members [*Boehner*, 1986] and several transgression-regression cycles of varying intensity [*Giles*, 1981]. The Green Oaks Formation includes all of Cycles 3 and 4, as well as the beginning of Cycle 5. It also includes seven more limestone/dolostone members, which each representing one of the transgression-regression cycles within this group [*Giles*, 1981; *Boehner*, 1986]. They alternate with the dominant siltstone and sandstone beds, with minor gypsum/anhydrite beds marking the transitions [*Giles*, 1981]. The seventh limestone/dolostone members is the last named one, and the last bed of the Green Oaks Formation. It marks the beginning of Cycle 5 [*Boehner*, 1986]. The remainder of Cycle 5 is the Watering Brook Formation. This formation no longer contains limestones nor dolostones, and is primarily silt- and sandstone with sulphate beds, which become thinner and less common towards the top of the formation [*Boehner*, 1986].

Of the ten formations within the Windsor group, six are present in core SB-1. The section of core examined covers all, or covers parts of, four of those formations: Stewiacke, MacDonald Road, Green Oaks, and Watering Brook.

Core SB-1

Pacific Coast Exploration (U.S. Borax) drilled core SB-1 (for location see Figure 2-1). It is 2928 ft deep and extends through the entirety of the Windsor Group into the Horton Group below [Boehner, 1986]. The uppermost 150 ft of the drill core were not recovered but consist of only overburden, which was not pertinent to this research. The core is stored in the Nova Scotia Core Library in Stewiacke.

The core records the five major transgression-regression cycles Giles (1981) identified and includes all fourteen limestone/dolostone members. While some of the salt deposits in the area are diapirs and are deformed, the halite horizons in core SB-1 were not affected by salt migration, and the strata are well bedded and well preserved [Gibling et al., 2008]. These were analogous to the halite beds Holt et al. performed fluid inclusion analyses on in order to establish seawater chemistry and conditions [2014]. The halite sections they studied are from 330 Ma and 335.5 Ma, and they found that the Mg/Ca ratio is higher in the younger section. See Figure 2-2 for the stratigraphy of the core in its geologic context.

Chapter 3 - Methods

Core Description

This study uses core SB-1 (Figure 3-1), which was drilled by U.S. Borax in 1976. The original core logging is in feet, rather than meters. While some publications have since used meters, including Giles [2009], not all have. To facilitate correlation between the data in this study and others, and most importantly, the original core, core logs, and core descriptions, imperial units have been used here. The core record extends from 166' to 2928', and the entirety is in storage at the Department of Natural Resources Core Library, in Stellarton, Nova Scotia.

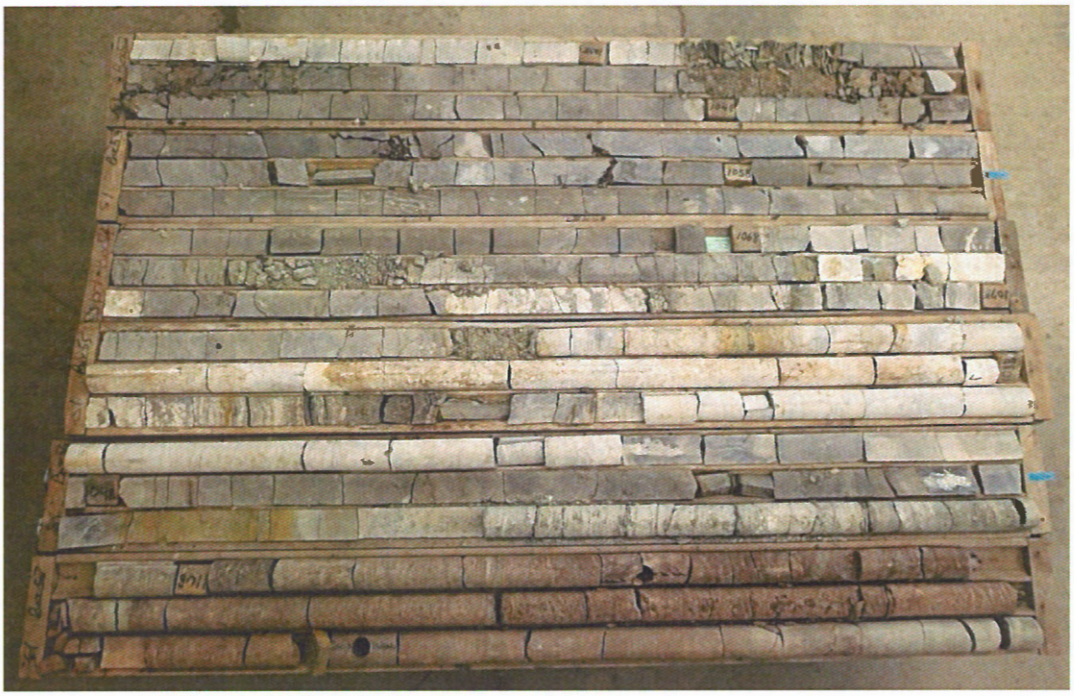

Figure 3-1 Photo of core from 1035-1120 ft depth. This photo shows the grey dolostone, the white (with minor blue) sulfate, and the red siltstone.

The focus of this study is on the upper section; the core description extends to 1805'. This length of core was stored on 4 pallets, holding a total of 93 core boxes, with ~20' of core in each box. I spent four days logging and sampling the core. The original core description from U.S. Borax was available. I took photos of the whole core, as in Figure 3-1, and collected a series of hand samples, as in Figure 3-2. Sampling was focused in and around the limestone members,

and avoided the siltstone beds. The sampled sections were cut with a saw on site and then labeled and bagged for further study.

Figure 3-2 Photo of sample CB-48, a coarse nodular anhydrite with a silty dolostone matrix; ruler for scale with centimeters denoted.

Polished Sections – Petrographic Descriptions

After sampling the core and returning to Halifax, I selected sub-areas of the samples for thin sectioning. The Dalhousie Thin Section Lab prepared polished thin sections from those samples. Each thin section was photographed using the Epson V600 scanners in the GIS lab. Additionally, the thin sections were studied in the Dalhousie University microscope lab, using a Nikon 50i transmitted-light microscope. The primary purpose of this was to select the best areas for the microprobe analysis and obtain a more detailed description of the mineralogy in each sample.

Microprobe Analysis

I collected back-scatter electron (BSE) images and x-ray maps using the JEOL 8200 Superprobe in the Robert M. MacKay Electron Microprobe Laboratory at Dalhousie University. Point analyses of mineral phases were also performed on the sections in order to determine localized chemical variations in Ca, Mg, Sr, and Ba content in carbonate and sulphate minerals, and to identify minerals that have been affected by diagenetic overprinting (e.g. dolomite with high Fe-content). These processes used the polished thin sections. The Superprobe operated at an

accelerating voltage of 15 kV and probe current of $1.00*10^{-8}$ A, with a minimum spot size of 5 μm. The low current and large spot size are due to the nature of these rocks; carbonates and evaporites burn more easily than harder rocks do. Quick Energy Dispersive Spectroscopy (EDS) analyses of prospective sample locations were performed to get an idea of the minerals present and to ensure microprobe analyses were performed on relevant minerals. The microprobe analysed for Ca, K, Mg, Sr, Mn, Pb, Ba, Na, Fe, P, and S.

The initial results are expressed in weight percent (Wt. %), but need to be converted to atom units. To do so, I modified the generic formula spreadsheet available from Brady and Perkins, [2015] to include the relevant elements. The equation this spreadsheet uses is as follows:

$$\left(\frac{Wt\%_e}{GFW_e}\right) * \left(\frac{\#O}{\sum\frac{Wt\%}{GFW}}\right) = atom\ unit_e \qquad \text{Equation 1.}$$

where Wt% is the weight percent, e is the element calculated for, GFW is the formula weight of that element's oxide, and #O is the number of oxygen atoms in that oxide.

X-Ray Fluorescence (XRF)

The Thermo Scientific Niton XL3t 950 GOLDD XRF at the Dalhousie XRF lab was used to analyse the hand samples. Analyses in mining mode take 180s and analyse the bulk composition of a $3mm^2$ spot. Each sample was analysed in 2 to 6 different places, depending on the length of the sample. The distance between analyses within a single sample was never more than three centimeters. The elements analysed were Mg, Ca, Sr, Ba, Fe, Mn, S, and Si. Plotting the results from these analyses with depth creates a chemical stratigraphy of the section.

Chapter 4 – Results

Sample Descriptions

There are 65 core samples from throughout the core; the largest spacing was around sixty feet and the smallest was less than one. The average spacing between samples was 15 feet, over half were within 10 feet of the next sample, and approximately three quarters of them were within 20 feet. I focused sampling within and around the limestone/dolostone members. See Figure 2-2 for core log with sample locations. There were several distinct textures visible in hand sample. As in Figure 3-2, most sulphate layers are composed of anhydrites, which are nodular, with a varying amount of either dolostone or siltstone matrix. In the bedded and massive anhydrites, there are wispy inclusions of silt and dolostone. In the massive anhydrites, these inclusions are random, whereas they follow roughly parallel lines in the bedded samples. Some of the anhydrite has a chicken-wire texture, as in Figure 4-3d. Chicken-wire texture can be primary or a product of diagenesis [*Scholle and Ulmer-Scholle*, 2003]. The carbonates were primarily packstone or wackestone, with some mudstone, after Dunham (1962). See Figure 4-2 for photos of more common textures in hand sample and Figure 4-3 for common thin section textures. See Appendix A: Sample Descriptions and Locations for a description of each sample.

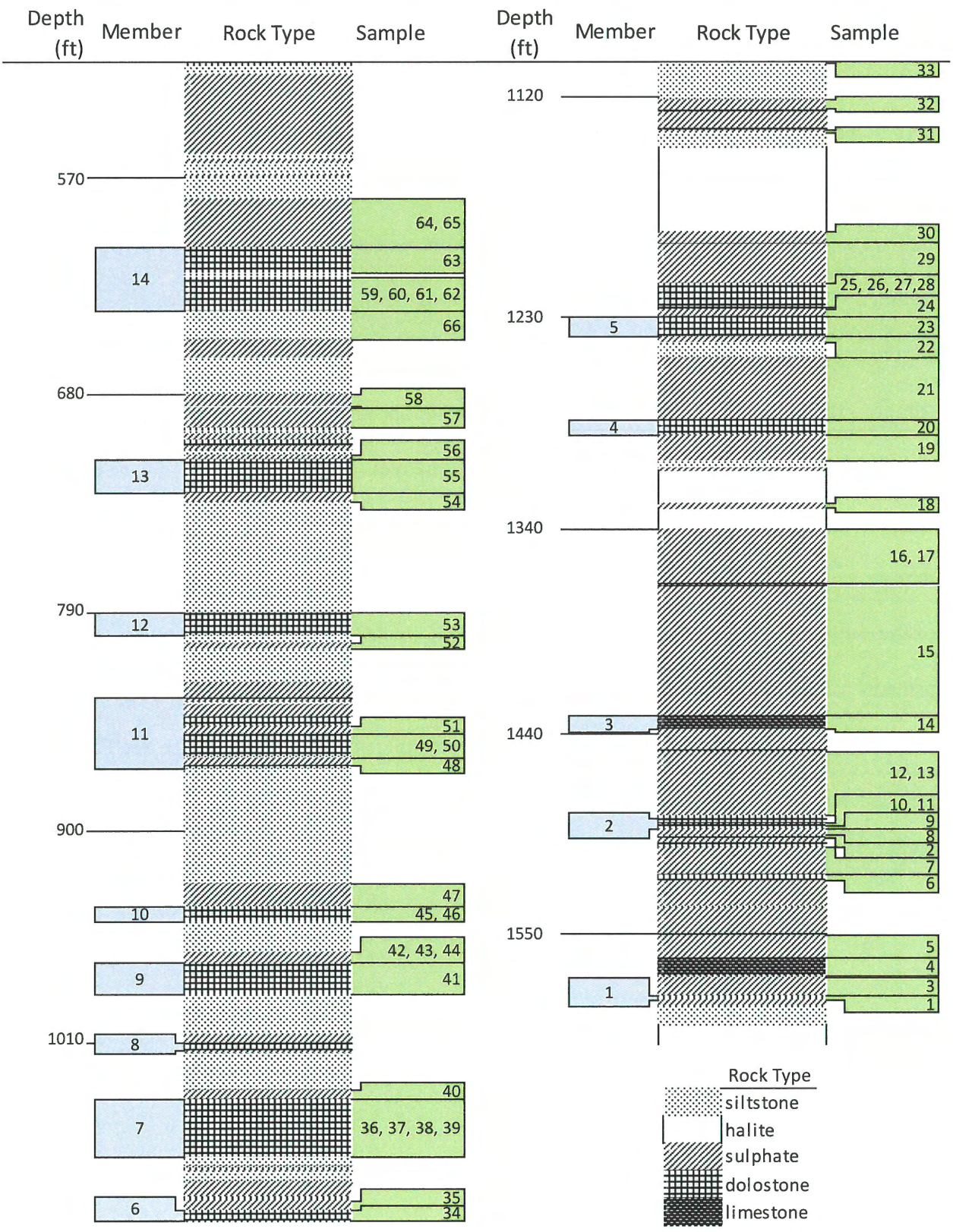

Figure 4-1 Core log with member and sample locations.

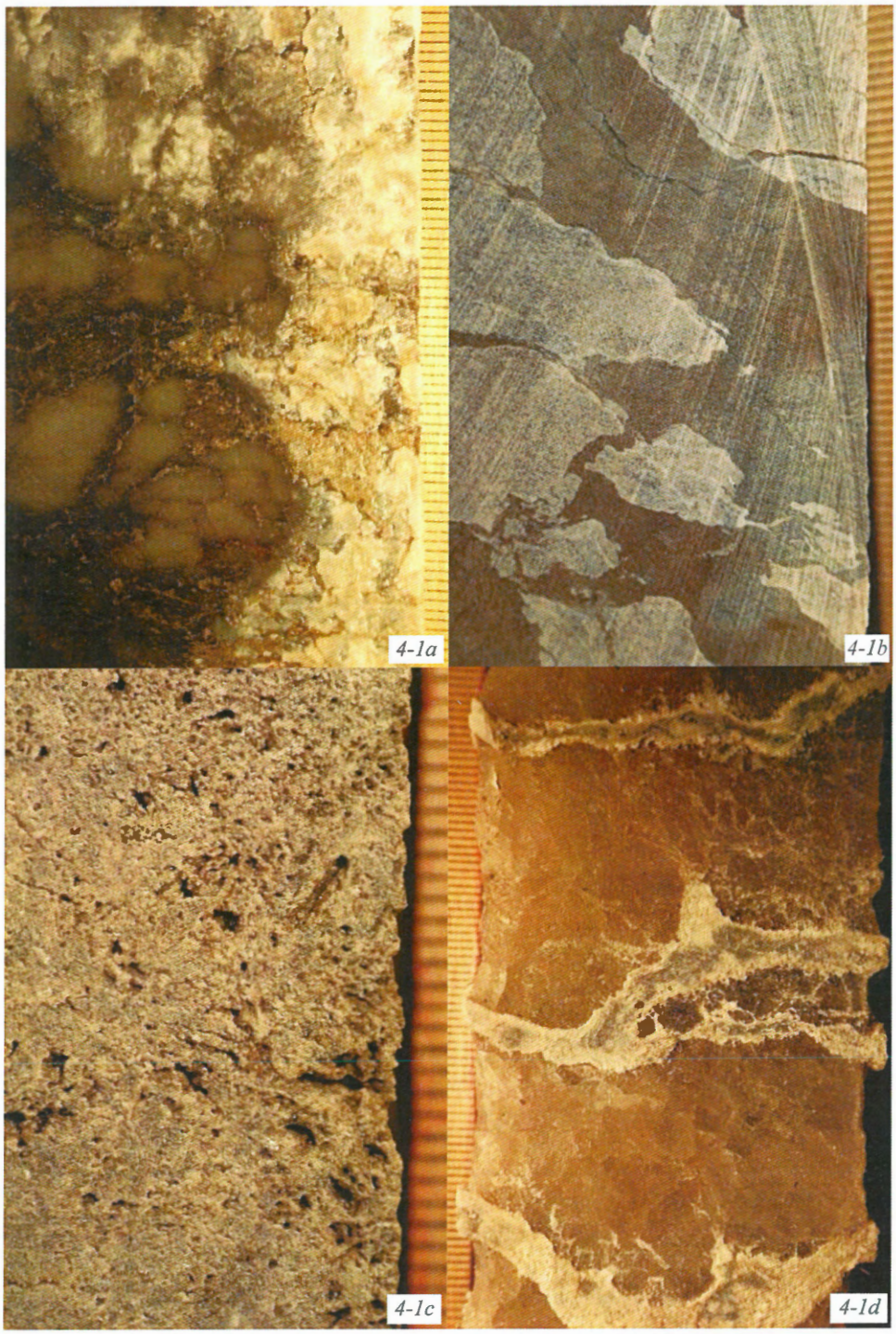

Figure 4-2 Photos of common textures in hand sample, ruler markings in millimeters. A) Interbedded sulphate and dolostone, with opaque, white sulphate on the right and darker dolostone on the left. B) Nodular sulphate in a silt and sandstone matrix. The siltstone is green and the sandstone is red. C) Fossiliferous limestone. D) Pink halite with interbedded white-grey anhydrite. This sample is from a halite bed analogous to the halite bed in core 153-3 where Holt et al. [2014] took the upper Asbian samples.

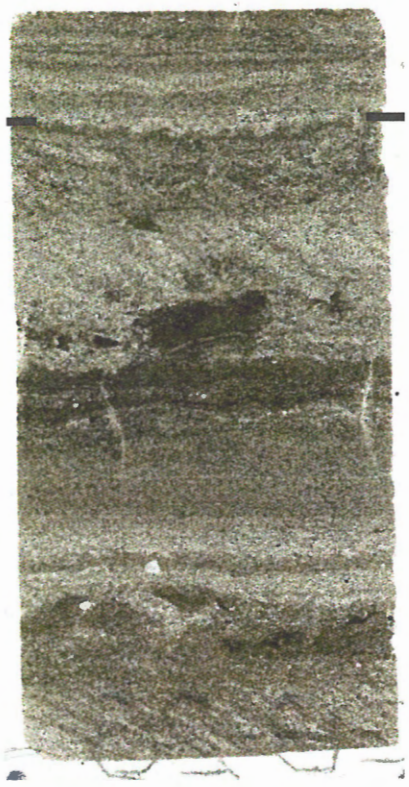

4-3a Sample CB-26

4-3b Sample CB-14

4-3c Sample CB-46

4-3d Sample CB-29

Figure 4-3 Thin section scans. FOV = 27mm and the top is up for all. A) Mudstone with waveforms visible between the black lines. B) Fossiliferous and bedded dolostone (packstone). C) Dolostone (mudstone) with bedding (dark) and sulphate nodules (light). D) Nodular anhydrite with chicken-wire texture.

Microprobe Data

I used the microprobe to analyse thin sections from samples 19, 20, 21, 45, 46, and 47. Samples 19, 20, and 21 are from a sulphate-dolomite-sulphate sequence and include the fourth dolostone member, as well as the sulphates on either side. Samples 45, 46, and 47 are from the tenth dolostone member and the sulphate that followed gradationally. These six samples include all the characteristic textures, except the massive anhydrites. Their different locations relative to major transgressions and their textural differences made them ideal for the more detailed microprobe analyses. Some of the mineral formulas based on the resultant microprobe data (Equation 1) are in Table 4-1. The results of all analyses are in Supplementary Document 1.

The amount of Ca, along with the presence or lack of Mg, indicate whether the grain was a calcite, dolomite, or sulphate. The Fe content is indicative of diagenesis. Figure 4-4 includes Ca, Mg, and Fe data from the calcite, dolomite, and anhydrite standards, as well as the data from the thin sections. The dolomite and sulphate results from the samples are indistinguishable from the standards. None of the thin section results were indicative of calcites, so this figure shows the calcite standard for reference only. The Ca value does not vary by more than 2.2 Wt. % within any of the groups. The dolostones plot on the left-hand side of the graph (Figure 4-4), with lower Ca, high (20±1.5 Wt. %) Mg, and high Fe. The Fe content was below 1 Wt. % with the exception of three points that plot around 3 Wt. %. The calcite standards plot on the right of the graph, with high Ca and little else. The sulphates plot in the middle, and have no Mg and little (<0.07) Fe.

	CaO	K2O	MgO	SrO	MnO	PbO	BaO	Na2O	FeO	P2O5	SO3	**Total**
Anhydrite	41.234	0	0	0.046	0	0	0	0	0	0.044	51.551	92.88
Dolomite	29.976	0.009	21.674	0.081	0.014	0.011	0	0	0	0	0	51.77
Calcite	55.744	0.002	0.013	0	0.036	0	0	0.014	0	0.021	0.019	55.85
CB19-08	41.485	0.024	0	0.118	0	0	0	0.012	0	0	53.765	95.40
CB20-09	28.873	0.237	19.649	0	0.166	0	0.024	0.027	0.593	0.026	0.006	49.60
CB21-01	41.488	0.016	0	0.208	0	0	0	0.046	0	0.001	52.925	94.68
CB45-13	29.873	0	20.950	0.004	0.183	0	0.043	0.005	0.193	0.058	0.029	51.34
CB46-05	40.608	0.015	0	0.204	0.026	0	0	0.019	0.016	0	53.054	93.94
CB47-11	40.963	0	0	0.019	0	0	0	0.011	0	0	52.919	93.91
	Ca	K	Mg	Sr	Mn	Pb	Ba	Na	Fe^{+2}	P	S	**No.O**
Anhydrite	1.101	0	0	0.001	0	0	0	0	0	0.009	2.892	4
Dolomite	2.984	0.001	3.002	0.009	0.001	0.000	0	0	0	0	0	6
Calcite	2.990	0.000	0.001	0	0.002	0	0	0.003	0	0.009	0.002	3
CB19-08	1.073	0.001	0	0.003	0	0	0	0.001	0	0	2.921	4
CB20-09	3.033	0.030	2.872	0	0.014	0	0.001	0.010	0.049	0.022	0.001	6
CB21-01	1.084	0.001	0	0.006	0	0	0	0.004	0	0.000	2.905	4
CB45-13	3.005	0	2.933	0.000	0.015	0	0.002	0.002	0.015	0.046	0.006	6
CB46-05	1.065	0.001	0	0.006	0.001	0	0	0.002	0.000	0	2.924	4
CB47-11	1.077	0	0	0.001	0	0	0	0.001	0	0	2.922	4

Table 4-1 Representative microprobe analysis with raw data and recalculated values.

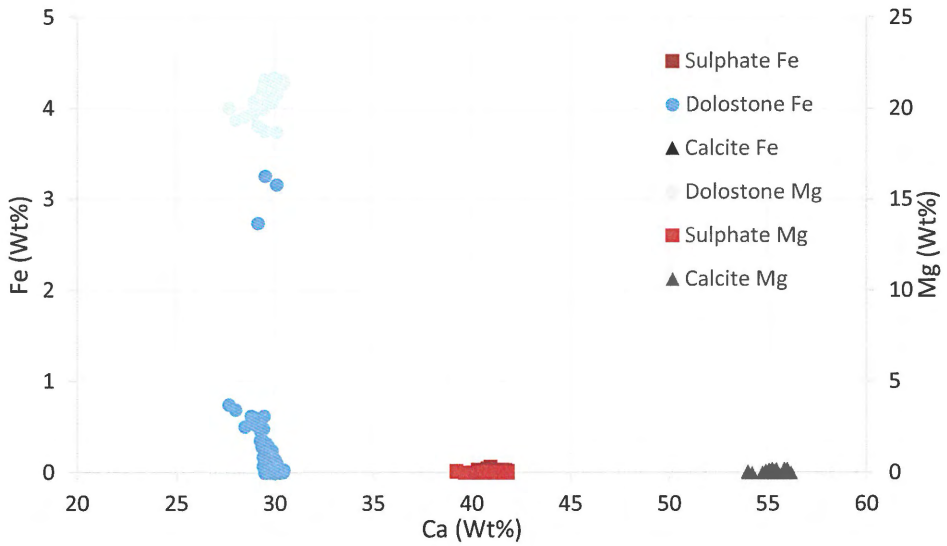

Figure 4-4 Graph of Fe (darker colours) and Mg (lighter colours) content against Ca content in all dolostone (blue circles), sulphates (red squares), and in the calcite standard (greyscale diamonds).

The Ca, Mg, and S trends are also visible in the x-ray maps. These maps provide more information on the distribution of different minerals within the sample by analysing for Ca, S, Mg, Sr, and Fe. Figure 4-5 shows the Ca, S, and Mg values for sample 46, which is a dolostone with interbedded sulphates. Where the S content is high, Ca is also high; this is characteristic of the sulphates. Where there is more Mg, the Ca values are lower; these areas are the dolostone. The Sr distributions follows the S distribution, and the Fe follows the Mg.

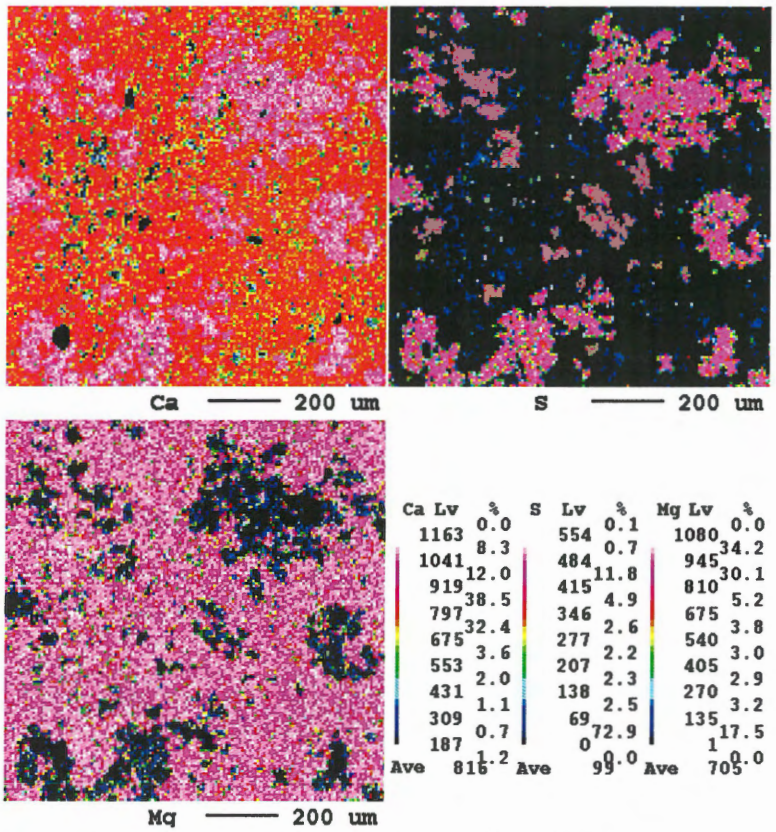

Figure 4-5 X-ray map of mixed dolostone and sulphate. From CB-46.

Some of the textures in thin section are clear in the x-ray maps, such as fine bedding in dolostone from CB-20 (Figure 4-7). Microprobe analysis of this sample was difficult, as the dolomite grains were interspersed with other, non-dolomitic grains that appeared identical in the different preview options. EDS analysis of those other grains identified them as being Si rich. In this map, the Ca lows correspond to lows in Mg, S, and Fe; they are therefore not minerals typical of these sequences. Those lows do correspond to high Sr values; based on this and the

EDS spectrums from the sample, it is likely a Sr rich silicate. Another visible texture is the chicken-wire texture in the anhydrite (Figure 4-6). Sample 21 is a sulphate with chicken-wire texture. The 'wires' have less Ca and S, and higher Fe, as in Figure 4-6, but also have lower Sr, and higher Mg.

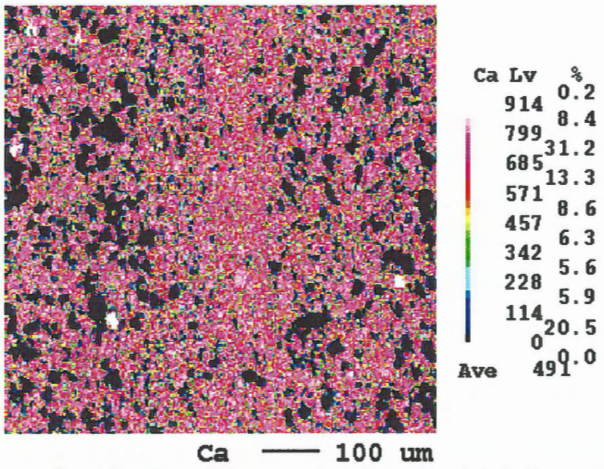

Figure 4-7 X-ray map of bedding in a dolostone (top is to the right). From sample CB-20

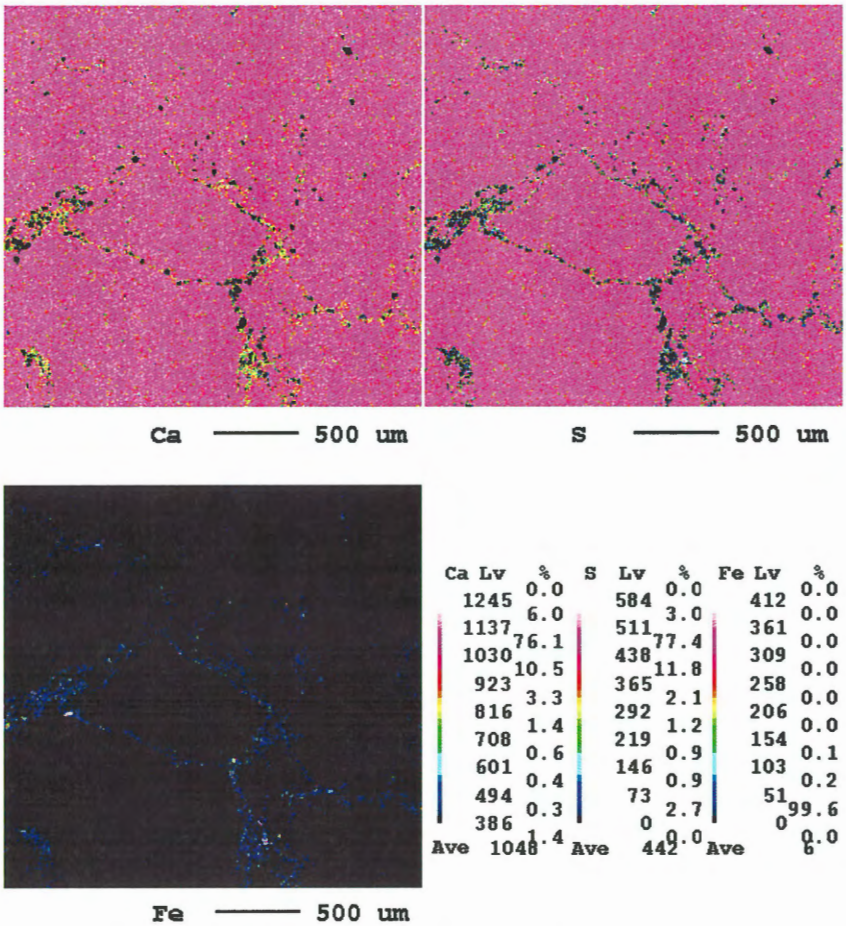

Figure 4-6 X-ray map of chicken-wire texture in sulphate. From sample CB-21

Other textures were visible in the x-ray maps, but not in thin section, such as the variability of Fe in some samples. In CB-45 (Figure 4-8, left) the broader areas with higher Fe correspond to small gaps between clusters of sulphate crystals, and the smaller wisps correspond to dolomitic regions. In CB-20, zones of higher Fe concentration either correspond to S-rich grains (likely Fe-sulphates) or do not correspond to other trends in the mapped elements.

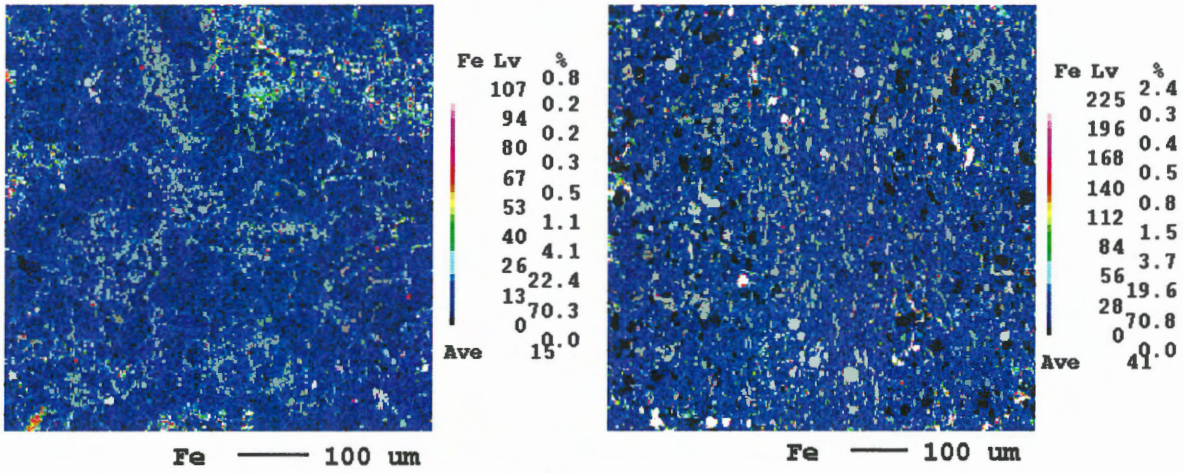

Figure 4-8 L X-ray maps: Left: Fe content in a fossiliferous dolostone (CB-45). Right: Fe content in the bedded dolostone (CB-20). Note: The maps use different Fe scales.

XRF Data

The XRF data includes analysis of Mg, Ca, Sr, Ba, Fe, Mn, S, and Si on all hand samples, except three whose surfaces were too rough to analyse accurately. Figure 4-9 shows the results of those analyses with depth. The Mg data show the cyclic nature of the deposit, with high Mg in the dolostones, and no detectable Mg in the sulphates (limit of detection (LOD) = ~3000ppm) and limestones. The samples from transitional sulphate to dolomite zones have intermediate values.

Likewise, the sulphates all have similar, high Ca values. The limestone samples were the only to have higher concentrations. The dolostone and transitional samples have variable Ca concentrations, though the dolostones show a positive trend from 1300 to 900 ft, where the values drop.

The Fe plot shows that iron content is lowest in the sulphates and highest in the dolomites. The sulphate samples at 868 and 1493 ft. and the uncategorized samples at 1038, 1220, 1365, and 1570 ft. with higher Fe are Ca-poor and rich in Si. Silicon is otherwise stable and present only in low concentrations. The peaks occur primarily in the dolostone samples and similarly correspond to Fe peaks and Ca lows in the same samples.

Sulphur concentrations are higher in the sulphates than the dolostones. Similarly to the Mg data, the S concentrations in the transitional samples lie in the middle. The data from sample 46, at 940 ft. depth, have higher S concentrations than the other dolomites from nearby.

The Ba plot shows a general negative trend, with increasing Ba with depth in the dolostones, and stable Ba in the sulphates.

The Sr values are higher in the sulphates than the dolostones and limestones. It is present only in relatively small concentrations in the dolomite samples. The amount of Sr in the sulphates increases by approximately 300 ppm from the bottom to around 900 ft, where it decreases by the same amount. It then begins to increase again from 800 ft. upward. The relatively low Sr values in the sulphate at 868 ft are in a sample with high Si and low Ca.

The Mn plot shows higher values in the dolostone and limestone than the sulphate, with the transitional samples in between. In the sulphates, there are samples with no detectable Mn throughout the core (LOD = ~33 ppm). However, the non-zero Mn values (minimum value = 50 ppm) increase with depth, from approximately 100 ppm around 600 ft to 960 ppm below 1200 ft. In the dolostones, values increase from approximately 500 ppm to 2000 ppm between 600 ft and 1200 ft. In the other samples, the Mn maximum of around 1500 ppm is also at depth; it follows the same decreasing trend as the other sample group.

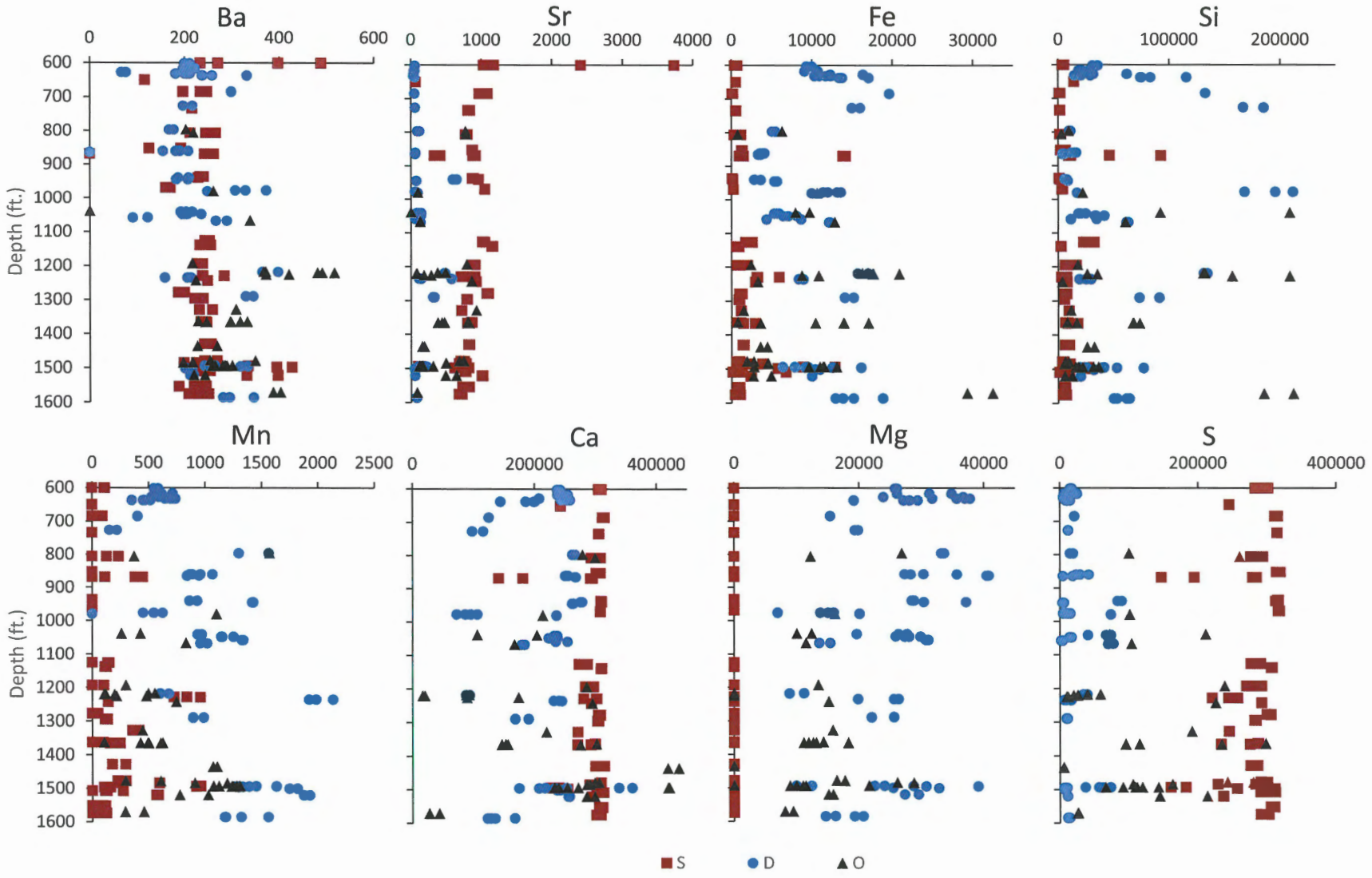

Figure 4-9 XRF data for Mg, Ca, Fe, S, Ba, Sr, Si, and Mn measured in ppm, with depth (ft). All graphs use the same y-axis and the same symbols indicating the dominant composition, where S = sulphate (red squares), D = dolostone (blue circles), and O = other (black triangles).

The ratios between the elements are more helpful than individual elements when investigating changes in paleo-temperature in the ocean (see Figure 4-10). The Mg/Ca fluctuates between 0 and 0.3 in the core. The sulphates invariably have no Mg. The Mg/Ca ratio in the dolomite samples only (Figure 4-11) range from 0.03 to 0.2 and, for samples from similar depths, vary by 0.05-0.01 for most of the core, resulting in a sawtooth pattern. In the lowest 100 ft of core, there is increased variability, with values ranging from 0.03 to 0.16. From 1300 to 700 ft, there is a steady positive trend, with a difference of ~0.05 from top to bottom of that section, with a maximum of 0.2 just below 700 ft. The Mg/Ca ratio above 700 ft is lower, with values between 0.1 and 0.15. There are two sample points from a silty dolostone sample, rich in organic matter, which had 0.21 and 0.29 ppm Mg/Ca, producing the spike at the bottom of the section.

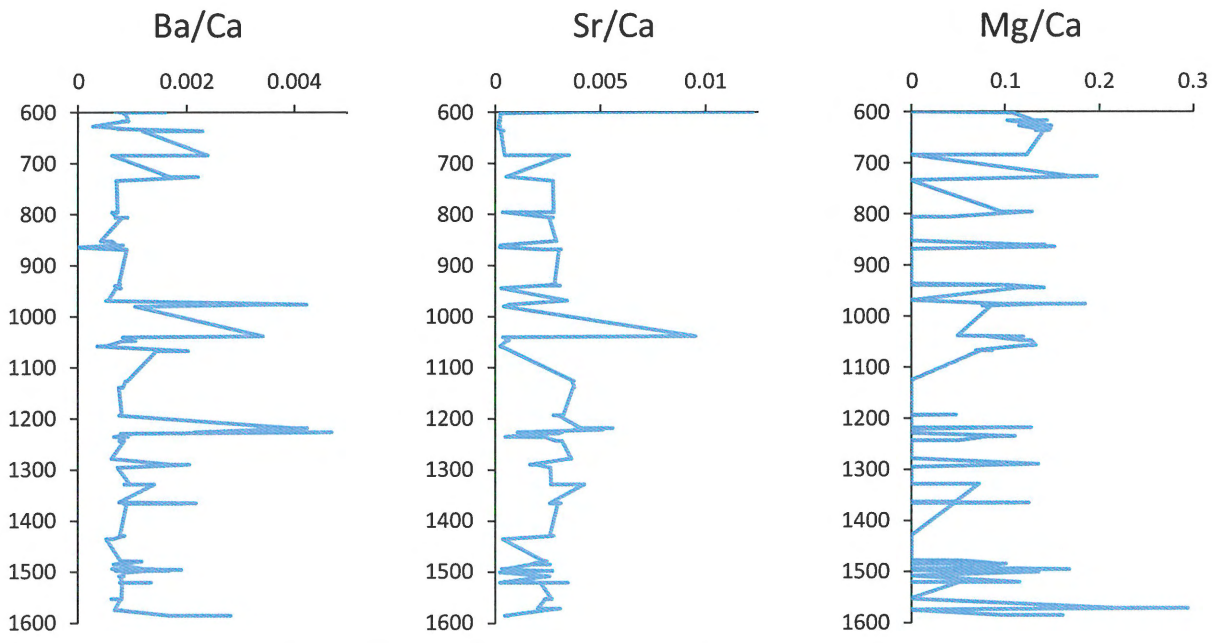

Figure 4-10 XRF element ratio data for all sample points in ppm.

The Ba/Ca and Sr/Ca graphs have a similar, but mirrored, pattern. In this case, the data from the sulphate samples is the most useful, since the others contain only low levels of Ba or Sr. The Ba/Ca ratio increases and the Sr/Ca has relatively consistent values until 1100 ft, at which

point they begin to decrease. Both are more varriable in the lowest 100 ft of the section.

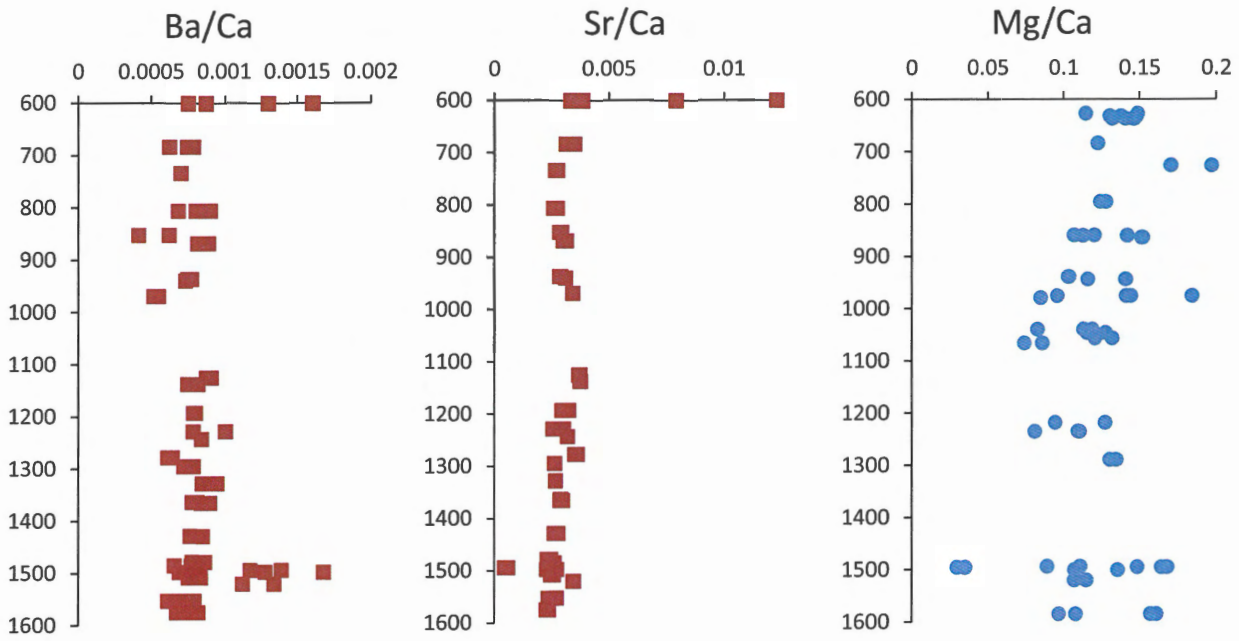

Figure 4-11 XRF data for the sulphates (red squares) or dolomites (blue circles) only.

Chapter 5 – Discussion

Diagenesis

The microprobe data show that there is Fe in the carbonate samples. Comparing the microprobe data and the XRF data in the same samples shows similar trends with both methods of analysis. This Fe is most likely due to diagenesis, based on the textures in the x-ray maps and the fact that seawater has very little Fe [*Moore*, 1989; *Morse and Mackenzie*, 1990].

The Fe content of the core varies between 0 and 20000 ppm, according to the XRF analysis. The variable values in the carbonate layers (e.g. Figure 4-8) are likely indicative of changes in the degree of diagenesis, with more diagenesis occurring in areas corresponding to high Fe values. The higher values are in the dolostones and in Si-rich samples. The anhydrite has lower Fe, with some spikes that correspond to samples just above transgression surfaces, which also have high Si. A greater terrigenous signal, corresponding to the transgression, would contribute more Fe due to the relative abundance of Fe-rich clay minerals.

In the sulphate samples, there are concentrations of Fe around sulphate nodules with chicken-wire texture (e.g. Figure 4-6). Chicken-wire texture can be primary (during the growth of anhydrite nodules they compress other material present) or through diagenesis (gypsum/anhydrite transformation) [*Scholle and Ulmer-Scholle*, 2003]. The presence of Fe in the carbonaceous 'wire' supports the second possibility, since again, there is little Fe in the seawater. In such circumstances, there is commonly O-isotope exchange, which obscures the original seawater signatures [*Al-Aasm and Packard*, 2000].

Given this record of diagenesis, it is possible that there have been changes to the elemental composition of this section. However, changes in the ratios of elements can still be useful if diagenesis occurred in rock, rather than water, dominated systems [*Cicero and*

Lohmann, 2001]. The determination of the rock-water interactions requires $\delta^{13}C$ data, which was not within the scope of this study. So long as $\delta^{13}C$ does not change, the Sr/Ca and Mg/Ca ratios should not have changed either [*Cicero and Lohmann*, 2001].

Seawater History

Mg/Ca

Different element ratios can reflect changes in the paleo-temperature of the ocean over that time period. Due to the sequence of deposition, the sulphate samples will be depleted in Mg. XRF analysis showed no detectable Mg in the sulphates. The other data points with lower ratios are from non-uniform dolostone samples with some sulphate, which would simultaneously lower the Mg and increase Ca, thereby decreasing the Mg/Ca ratio. In general, ratio values from the same or nearby samples vary by ~0.05 to 0.1 ppm Mg/Ca. While some of that variation could be due to instrument error, the consistency of the variability suggests that a natural process is responsible for the main signal. These variations are similar in frequency to the transgressive-regressive cycles in Giles [1981].

The Mg/Ca ratios in samples that contain Mg and do not have obvious sulphates mixed in have a wide range of values at depth (>1475 ft). The values from this part of the core are also relatively high (~0.2). The highly variable values at the bottom of the section correspond to the shorter transgressive-regressive cycles Giles [2009] identified at the beginning of Cycle 2. At this time (Asbian), 100 ka orbital forcings dominated and caused the transgressive-regressive cycles. After this period, during the Brigantian, the 400 ka cycles dominated, leading to longer transgressive-regressive cycles [*Giles*, 2009]. In the last 50 ft of core in this section, the rate of variation is similar to that at the bottom of the section and the transgressive-regressive cycles are shorter.

There is a general increase from ~0.15 to 0.25 in Mg/Ca up-core. While there are only

two data points from around 725 ft, they are both higher than the surrounding points. Values decrease slightly in the last 50 ft. of the section. Since the Mg/Ca ratio increases with increasing temperature, the seawater may have warmed throughout deposition represented by the section of core from 1500 to 725 ft, and then experienced a general cooling trend after that.

Holt et al.'s 2014 study showed higher Mg/Ca ratios at 330 Ma than 335.5 Ma. Core depths of ~600 ft and 1200 ft correspond to those ages, and the Mg/Ca ratios from this study for those depths do show the same relative change. This study looked at changes in this ratio in more detail, and therefore shows evidence of fluctuations on a smaller scale.

Ba/Ca

Another temperature-dependant ratio is the Ba/Ca ratio, however, this ratio also depends on the relative concentrations in the seawater. If the Ba and Ca values show a linear trend with respect to each other, this would indicate system dominated by changes in the seawater composition. If they do not follow a linear trend, the temperature dependant signal is dominant. There is a negative, linear relationship between Ba and Ca in the dolomite samples (as Ca increases, Ba decreases), therefore, the seawater composition was the likely primary influence of the Ba/Ca ratio in these samples. In the sulphate samples, however, Ba varries independently from Ca, meaning any changes are more likely due to temperature than variations in seawater concentration. There are two outliers from one sample that both have very low Ca, high Si, and high Mg, and sit just above a siltstone layer. The stronger terrigenous input in this sample excludes it from the Ba/Ca ratio analysis.

Similarly to the Mg/Ca ratio in the dolostones, the Ba/Ca ratio in the sulphates is highly variable below 1475 ft. After this point, the values are stable, with highs around 1150 and 600 ft, and lows around 725 ft. The increases and decreases between these highs and lows are not

dramatic, but they are the inverse of the Mg/Ca ratio, which supports the interpretation of larger scale temperature changes.

Sr/Ca

The last temperature dependant ratio is Sr/Ca. It is also more variable at the top and bottom of the section. In the sulphates, it increases and decreases at the same depths as the Ba/Ca ratios do. However, in the dolostones, the Sr/Ca ratio does the opposite, and accords well with the Mg/Ca ratio instead. The distribution coefficient of Sr is higher, at a given temperature, in calcite with more magnesium [*Morse and Mackenzie*, 1990]. For a given Mg concentration, the temperature dependence remains the same. It makes sense then, that the Sr/Ca ratio in the dolostones would reflect the Mg/Ca ratio rather than a temperature dependant one, since the Mg/Ca changes on a shorter timescale than the temperature trends throughout the core.

Conclusions

In general, the Mg/Ca ratios determined in this study follow the same increasing trend as in Holt et al. [2014]. This study also looked at changes in this ratio in more detail, and therefore shows evidence of fluctuations on a smaller scale. The Sr/Ca and Ba/Ca ratios echo these changes in the Mg/Ca ratio. As an ensemble, the trends in the Mg/Ca, Sr/Ca, and Ba/Ca ratios suggest that the ocean cooled during deposition of the material from 1450 to 1150 ft (~336.3-335.3 Ma) and 725 ft to the top (~331.5-330 Ma) of the study section, and warming between 1150 and 725 ft (~335.3-331.5Ma). They also show shorter-scale variability coincident with the local transgressive-regressive cycles and their shift from 100 ka cycles to 400 ka cycles.

The presence of Fe around anhydrite nodules and fossils, in addition to Fe in the dolomite, suggests some diagenesis has occurred. Given this, it is possible that there have been changes to the elemental composition of this section. Since this study did not investigate whether

diagenesis occurred in a rock or water dominated system in this section of core, further study is required. Establishing which system controlled the diagenesis will determine if the trends in element ratios are primary or not.

References

Al-Aasm, I. S., and J. J. Packard (2000), Stabilization of early-formed dolomite: a tale of divergence from two Mississippian dolomites, *Sediment. Geol.*, *131*, 97–108.

Allen, J. P., C. R. Fielding, M. C. Rygel, and M. R. Gibling (2013), Deconvolving Signals of Tectonic and Climatic Controls From Continental Basins: An Example From the Late Paleozoic Cumberland Basin, Atlantic Canada, *J. Sediment. Res.*, *83*(10), 847–872, doi:10.2110/jsr.2013.58.

Andreasen, G., and M. Delaney (2006), Calcite Sr/Ca ratios as paleoceanographic tracer and diagenetic indicator, University of California Santa Cruz.

Boehner, R. C. (1986), Salt and Potash Resources in Nova Scotia, *Nov. Scotia Dep. Mines Energy Bull.*, *ME 005*, 346.

Boggs, S. J. (2012), *Principles of Sedimentology and Stratigraphy*, 5th ed., Pearson Education, Inc., Upper Saddel River.

Brady, J., and D. Perkins (2015), Mineral Formulae Recalculation, Available from: http://serc.carleton.edu/research_education/equilibria/mineralformulaerecalculation.html (Accessed 20 January 2016)

Calder, J. H. (1998), The Carboniferous evolution of Nova Scotia, *Geol. Soc. London, Spec. Publ.*, *143*, 261–302, doi:10.1144/GSL.SP.1998.143.01.19.

Carpenter, J., and A. Arbor (1992), Sr / Mg ratios of modern marine calcite : Empirical indicators of ocean chemistry and precipitation rate, , *56*, 1837–1849.

Cicero, A. D., and K. C. Lohmann (2001), Sr/Mg variation during rock-water interaction: implications for secular changes in the elemental chemistry of ancient seawater, *Geochim. Cosmochim. Acta*, *65*(5), 741–761, doi:10.1016/S0016-7037(00)00594-9.

Cohen, A. L., and G. A. Gaetani (2010), Ion partitioning and the geochemistry of coral skeletons: solving the mystery of the vital effect, in *Ion partitioning in ambient-temperature aqueous systems*, edited by H. Stoll, pp. 377–397.

Dunham, R. J. (1962), Classification of carbonate rocks according to depositional texture, in *Classification of carbonate rocks*, edited by W. E. Ham, pp. 108–121, American Association of Petroleum Geologists Memoir. 1, Tulsa, OK.

Gibling, M. R., N. Culshaw, M. C. Rygel, and V. Pascucci (2008), *The Sedimentary Basins of the United States and Canada*, Sedimentary Basins of the World, Elsevier.

Giles, P. S. (1981), Major transgressive-regressive cycles in Middle to Late Visean rocks of Nova Scotia, *Nov. Scotia Dep. Mines Energy*, 81–82.

Giles, P. S. (2009), Orbital forcing and Mississippian sea level change : time series analysis of marine flooding events in the Viséan Windsor Group of eastern Canada and implications for Gondwana glaciation, *Bull. Can. Pet. Geol.*, *57*(4), 449–472.

Gornitz, V. (2009), Mineral Indicators of Past Climates, in *Encyclopedia of Paleoclimatology and Ancient Environments*, edited by V. Gornitz, Springer, Dordrecht, The Netherlands.

Hasiuk, F. J., and K. C. Lohmann (2010), Application of calcite Mg partitioning functions to the reconstruction of paleocean Mg/Ca, *Geochim. Cosmochim. Acta*, *74*(23), 6751–6763, doi:10.1016/j.gca.2010.07.030.

Hem, J. D. (1985), EVALUATION OF WATER COMPosition, in *Study and Interpretation of the Chemical Characteristics of Natural Water*, pp. 42–57, UNITED STATES GOVERNMENT PRINTING OFFICE.

Hibbard, J., and J. W. F. Waldron (2009), Truncation and translation of Appalachian promontories: Mid-Paleozoic strike-slip tectonics and basin initiation, *Geology*, *37*(6), 487–

490, doi:10.1130/G25614A.1.

Holt, N. M., F. J. G. Veigas, T. K. Lowenstein, T. K. Lowenstein, P. S. Giles, N. M. Holt, J. Garcı, and S. Williams-stroud (2014), The major-ion composition of Carboniferous seawater, *Geochim. Cosmochim. Acta*, *134*, 317–334, doi:10.1016/j.gca.2014.03.009.

Jutras, P., R. J. Ryan, and R. Fitzgerald (2006), Gradual encroachment of a rocky shoreline by an invasive sea during the Mississippian at the southeastern margin of the Maritimes Basin, Nova Scotia, Canada, *Can. J. Earth Sci.*, *43*(8), 1183–1204, doi:10.1139/e06-094.

Lopez, O., P. Zuddas, and D. Faivre (2009), The influence of temperature and seawater composition on calcite crystal growth mechanisms and kinetics: Implications for Mg incorporation in calcite lattice, *Geochim. Cosmochim. Acta*, *73*(2), 337–347, doi:10.1016/j.gca.2008.10.022.

Lugli, S. (2009), Evaporites, in *Encyclopedia of Paleoclimatology and Ancient Environments*, edited by V. Gornitz, pp. 321–324, Springer, Dordrecht, The Netherlands.

Moore, C. H. (1989), *Carbonate Diagenesis and Porosity*, Elsevier Science, Amsterdam, NL.

Morse, J. W., and M. L. Bender (1990), Partition coefficients in calcite: Examination of factors influencing the validity of experimental results and their application to natural systems, *Chem. Geol.*, *82*, 265–277, doi:10.1016/0009-2541(90)90085-L.

Morse, J. W., and F. T. Mackenzie (1990), *Geochemistry of Sedimentary Carbonates*, Elsevier Science, Amsterdam, NL.

Murphy, J. B., J. W. F. Waldron, D. J. Kontak, G. Pe-Piper, and D. J. W. Piper (2011), Minas Fault Zone: Late Paleozoic history of an intra-continental orogenic transform fault in the Canadian Appalachians, *J. Struct. Geol.*, *33*(3), 312–328, doi:10.1016/j.jsg.2010.11.012.

St. Peter, C. (1993), Maritimes Basin evolution: key geologic and seismic evidence from the

Moncton Subbasin of New Brunswick, *Atl. Geol.*, *29*(3), doi:10.4138/2010.

Rimstidt, J. D., A. Balog, and J. Webb (1998), Distribution of trace elements between carbonate minerals and aqueous solutions, *Geochim. Cosmochim. Acta*, *62*(11), 1851–1863, doi:10.1016/S0016-7037(98)00125-2.

Salminen, R. (Ed.) (2005), *FOREGS Geochemical Atlas of Europe*.

Schenk, P. E., R. Matsumoto, and P. H. Bitter (1994), Loch Macumber (early Carboniferous) of Atlantic Canada, *J. Paleolimnol.*, *11*(2), 151–172, doi:10.1007/BF00686863.

Scholle, P. A., and D. S. Ulmer-Scholle (2003), *A Color Guide to the Petrography of Carbonate Rocks: Grains, Textures, Porosity, Diagenesis*, edited by John C. Lorenz, American Association of Petroleum Geologists Memoir. 77, Tulsa, OK.

Shen, C.-C., T. Lee, C.-Y. Chen, C.-H. Wang, C.-F. Dai, and L.-A. Li (1996), The calibration of D[Sr/Ca]versus sea surface temperature relationship for Porites corals, *Geochim. Cosmochim. Acta*, *60*(20), 3849–3858, doi:10.1016/0016-7037(96)00205-0.

Appendix

Appendix A: Sample Descriptions and Locations

No.	Depth (ft)		Rock Type	Classification	Notes	Thin Section
	Start	End				
1	1584.5	1584.8	dolostone	packstone		no
2	1500.3	1500.4	dolostone	packstone		no
3	1574.1	1574.3	anhydrite	nodular anhydrite	fine, chicken-wire texture	no
4	1570.5	1570.6	dolostone	mudstone	Laminated, lots of OM	no
5	1552	1552.4	anhydrite	nodular anhydrite	fine, bedding (strike and/or dip changes at midpoint)	no
6	1519.9	1520.2	anhydrite	massive anhydrite	silt matrix	yes
7	1507.6	1507.9	anhydrite	massive anhydrite	wispy silts	yes
8	1497	1497.1	anhydrite	nodular anhydrite	coarse	no
9	1494.9	1495.1	dolostone	wackestone	massive, halite inclusions	no
10	1493.3	1493.5	limestone	packstone	oncolites	no
11	1493.5	1494.0	dolostone	packstone		no
12	1484.0	1484.5	anhydrite	nodular anhydrite	fine, chicken-wire texture	no
13	1477.8	1478.0	anhydrite	nodular anhydrite	coarse, chicken-wire texture	no
14	1435.0	1435.3	limestone	packstone		yes
15	1428.3	1428.5	anhydrite	nodular anhydrite		yes
16	1365.0	1365.5	anhydrite	bedded	halite vein	no
17	1363.0	1363.2	anhydrite	nodular anhydrite	fine	no
18	1327.7	1327.8	anhydrite	nodular anhydrite	fine, halite vein	no
19	1294.6	1294.8	anhydrite	bedded anhydrite		yes
20	1289.0	1289.1	dolostone	mudstone		yes
21	1277.4	1277.6	anhydrite	nodular anhydrite	chicken-wire texture	yes
22	1242.9	1243.1	anhydrite	nodular anhydrite	silt matrix	no
23	1234.7	1235.0	dolostone	wackestone		no
24	1228.3	1228.6	anhydrite	nodular anhydrite	silt matrix	no
25	1225.7	1225.8	dolostone	wackestone		no
26	1222.8	1223.1	dolostone	mudstone	wave forms	yes
27	1220.5	1220.6	dolostone	mudstone		no
28	1217.6	1217.9	dolostone	wackestone	anhydrite vein	no
29	1206.9	1207.0	anhydrite	nodular anhydrite	chicken-wire texture	yes
30	1192.8	1193.1	anhydrite	nodular anhydrite	wispy silts	no
31	1137.9	1138.0	anhydrite	massive anhydrite		no
32	1125.3	1125.5	anhydrite	nodular anhydrite	chicken-wire texture	no
33	1102.5	1102.6	anhydrite	nodular anhydrite	chicken-wire texture	yes
34	1098.5	1098.6	dolostone	wackestone		yes
35	1095.3	1095.5	anhydrite	massive anhydrite	wispy silts	yes
36	1066.5	1066.6	dolostone	packstone		no

37	1057.0	1057.2	dolostone	packstone	high to lower silt transition	yes
38	1047.0	1047.2	dolostone	wackestone	nodular anhydrite	no
39	1040.0	1040.2	dolostone	wackestone		no
40	1037.8	1038.0	anhydrite	nodular anhydrite beds with wackestone	crossbeds	yes
41	984.5	984.7	dolostone	wackestone		yes
42	979.5	979.6	dolostone	wackestone		no
43	976.2	976.3	dolostone	wackestone		no
44	968.4	968.5	anhydrite	nodular anhydrite	chicken-wire texture	yes
45	944.0	944.2	dolostone	packstone		yes
46	939.0	939.2	dolostone	wackestone with anhydrite nodules	bedding	yes
47	936.0	936.3	anhydrite	nodular anhydrite	mudstone matrix	yes
48	868.4	868.5	anhydrite	nodular anhydrite	mudstone matrix	no
49	864.0	864.2	dolostone	packstone		yes
50	860.0	860.2	dolostone	wackestone		no
51	852.0	852.2	anhydrite	nodular anhydrite	chicken-wire texture	yes
52	806.5	806.7	anhydrite	massive anhydrite		no
53	796.0	796.2	dolostone	wackestone		no
54	734.0	734.1	anhydrite	bedded anhydrite		yes
55	726.2	726.4	dolostone	wackestone		yes
56	713.0	713.1	anhydrite	bedded anhydrite		yes
57	693.0	693.1	anhydrite	massive anhydrite		no
58	684.0	684.3	anhydrite	nodular anhydrite	coarse, chicken-wire texture	no
59	637.0	637.3	dolostone	packstone		no
60	632.0	632.3	dolostone	wackestone		no
61	627.0	627.3	dolostone	packstone		yes
62	621.8	622.0	dolostone	packstone		yes
63	617.0	617.2	dolostone	wackestone		no
64	602.0	602.2	anhydrite	wackestone	interlaminated in anhydrite	no
65	598.5	598.6	anhydrite	bedded anhydrite		yes